STM JOURNALS

Journal of
Polymer & Composites

ISSN: 2321-2810 (Online)
ISSN: 2321-8525 (Print)
Volume 13, Special Issue 6, 2025
DOI (Journal): 10.37591/JoPC

https://journals.stmjournals.com/jopc

Research JoPC

Fabrication and Assessment of Tribological Performance of Nickel-Graphene-MXene Hybrid Nano-composites

Shams Tabrez[1], Sudesh Singh[2,*], Vineet Kumar[3], Kumresh Kumar Gaur[4], Avinash Ravi Raja[5]

Abstract

As industries such as aerospace, automotive, defence, and electronics demand materials with superior wear resistance, high strength, and thermal stability, traditional metals are reaching their performance limits. Hybrid nanocomposites offer a pathway to meet these stringent requirements. In this study, novel Nickel-Graphene-MXene hybrid nanocomposites were fabricated using a powder metallurgy route, incorporating varying weight percentages (up to 2 wt.%) of MXene and 1 wt.% graphene nanosheets into a nickel matrix and evaluated for their tribological performance. Comprehensive characterization using FTIR, XRD, Raman spectroscopy, and FESEM-EDS confirmed the uniform dispersion of reinforcements and successful phase integration. Tribological performance was assessed under dry sliding conditions against a Si3N4 ball at room temperature, with results showing a significant reduction in both the friction coefficient and specific wear rate upon the addition of graphene and MXene. The composite containing 2.0 wt.% MXene (NG1M2.0) exhibited the best performance, achieving a ~61% reduction in the friction coefficient and an ~85% decrease in wear rate compared to pure nickel. Enhanced performance was attributed to the formation of stable tribo- and transfer films, which minimized direct contact and wear. These findings highlight the promising potential of Nickel-Graphene-MXene composites for advanced applications requiring superior wear resistance and mechanical durability.

Keywords: Nickel, Graphene, MXene, Metal matrix composite, Wear.

***Author for Correspondence**
Sudesh Singh

[1]Research Scholar, Department of Mechanical Engineering, Sharda School of Engineering and Science, Sharda University, Greater Noida, Uttar Pradesh, India
[2]Assistant Professor, Department of Mechanical Engineering, Sharda School of Engineering and Science, Sharda University, Greater Noida, Uttar Pradesh, India
[3]Associate Professor, Department of Mechanical Engineering, Sharda School of Engineering and Science, Sharda University, Greater Noida, Uttar Pradesh, India
[4]Scientist F, Defence Research and Development Organization, Lucknow Road, Timarpur, Delhi, India
[5]Assistant Professor, Department of Mechanical Engineering, PDPM Indian Institute of Information Technology Design & Manufacturing Jabalpur, Madhya Pradesh, India

Received Date: August 14, 2025
Accepted Date: August 28, 2025
Published Date: October 25, 2025

Citation: Shams Tabrez, Sudesh Singh, Vineet Kumar, Kumresh Kumar Gaur, Avinash Ravi Raja. Fabrication and Assessment of Tribological Performance of Nickel-Graphene-MXene Hybrid Nano-composites. Journal of Polymer & Composites. 2025; 13(Special Issue 6): S780–S798p.

INTRODUCTION

As science and technology continue to evolve, there is an increasing demand for designing systems that offer lower friction and wear, higher strength-to-weight ratios, and the ability to perform under complex and demanding conditions. This includes applications in the metalworking (machining and forming), automotive, power generation, military, aerospace, and marine industries [1,2]. However, conventional lubricants degrade rapidly under extreme operating conditions, making them ineffective in many high-performance applications. As a result, researchers are compelled to develop novel materials and lubrication strategies capable of maintaining tribological stability in harsh environments [3–5]. Friction and wear at sliding interfaces in mechanical systems are major causes of energy

© STM Journals 2025. All Rights Reserved

loss and material degradation, often leading to premature system failure [6–11]. To mitigate this, significant attention has been directed toward 2D/layered materials, which have emerged as promising candidates for solid lubrication in tribological applications [12,13]. Among them, graphene stands out due to its exceptional physical, thermal, mechanical, and electrical properties, particularly in multilayer graphene, which offers enhanced wear resistance [14,15].

The reliability and longevity of components, directly affected by friction, lubrication, and wear, are of paramount importance in contemporary civilization [9]. The use of multilayer graphene (MLG) as a solid lubricant in composites is gaining traction due to its cost-effectiveness, excellent lubricating behavior, and ease of dispersion within metal matrices. With the increasing concerns over the depletion of non-renewable energy resources such as coal and petroleum, reducing friction losses in critical sectors like transportation and manufacturing becomes imperative [16]. Accordingly, the development of high-performance solid lubricating materials, particularly those based on 2D materials like graphene, is a key focus for enhancing energy efficiency and durability in different areas [17,18]. Extensive research has demonstrated graphene's effectiveness in reducing wear and friction, both as a standalone material and as an additive in composite systems [19]. A recent breakthrough in this domain is the realization of macroscale superlubricity through the combination of graphene with other 2D materials [20,21].

MXenes, a relatively new family of 2D transition metal carbides and nitrides first reported in 2011, have also shown great promise for tribological applications. In particular, Ti_3C_2-MXene has demonstrated excellent potential as a solid lubricant [22,23]. Incorporating MXene into polymer composites, such as ultra-high molecular weight polyethylene (UHMWPE), has resulted in notable reductions in friction and adhesive wear [24]. While several studies have highlighted MXene's tribological potential, limited studies have been focused on exploring its synergistic effects with other 2D lubricants in the case of hybrid metal matrix composites [25–27].

Recent studies on Ni_3Al-based alloys reinforced with multilayer graphene (MLG) and Ti_3SiC_2 have demonstrated excellent tribological properties, showing substantial reductions in both friction and wear due to the synergistic effects of these hybrid reinforcements [28]. The incorporation of MXene into various matrices remains a growing area of interest, not only for its tribological benefits but also for its ability to enhance mechanical properties such as hardness and fracture toughness, particularly when combined with oxide modifiers like Y_2O_3 and Al_2O_3 [18,23,29].

Investigations into MXene phase modifications with such oxides have revealed that even a modest addition of MXene can significantly improve the mechanical behavior of ceramics like silicon carbide. During sintering, the MXene phase tends to oxidize, forming flake-like carbon structures with disordered graphite characteristics. The application of sol-gel techniques to deposit oxide layers (Al_2O_3/Y_2O_3) onto MXene surfaces has led to improved hardness and fracture toughness of the resulting composites. However, further research is needed to fully explore the potential of these surface-modified MXenes [29]. Additionally, Ni_3Al-MXene composites with varying MXene concentrations have shown that increasing MXene content enhances hardness while reducing density. Notably, incorporating 20 wt.% MXene into the Ni_3Al matrix resulted in a 93% reduction in friction and wear rate [30].

Despite these advancements, the synergistic lubricating effects of MXene and Graphene in nickel matrix composites at room temperature have been scarcely studied. This gap is particularly relevant for aerospace applications, where exceptional anti-friction and anti-wear characteristics are essential. Therefore, this work aims to investigate the tribological behavior and wear mechanisms of Nickel-Graphene-MXene composites under dry sliding conditions at room temperature. In the current study, Ni-based composites were synthesized using conventional powder metallurgy techniques involving uniaxial pressing and high-temperature sintering. A fixed amount of graphene (1 wt.%) and varying

© STM Journals 2025. All Rights Reserved

amounts of MXene (0.5 wt.%, 1.0 wt.%, 1.5 wt.%, and 2.0 wt.%) were incorporated into the nickel matrix to fabricate self-lubricating Nickel-Graphene-MXene composites. Comprehensive characterization of the composites was carried out using Fourier-transform infrared spectroscopy (FTIR), Raman spectroscopy, X-ray diffraction (XRD), and 3D optical profilometry. Surface morphology and elemental distribution were analyzed through field emission scanning electron microscopy (FESEM) and energy-dispersive X-ray spectroscopy (EDS). The tribological performance was evaluated using a ball-on-disk tribometer under unidirectional sliding against a silicon nitride (Si_3N_4) counter-face. This study provides significant insights into the relationship between microstructural features and tribological behavior, contributing to the development of high-performance, self-lubricating nickel-based composites for advanced engineering applications.

EXPERIMENTAL DETAILS

Raw Materials and Synthesis of Nickel-Graphene-MXene Hybrid Composites

Nickel Powder (Purity 99.5%, 200 mesh) and MXene-$Ti_3C_2T_x$ Powder (Purity 99.9%, APS < 100nm) were supplied by Loba Chemie PVT, India, and Nanoshel Limited, UK, respectively. Graphene powder (99%, average lateral size ~1 µm, thickness ~5-10 nm) was provided by Adnano Technologies Pvt Ltd, India. The field emission scanning electron microscope (FESEM) images of the powders used in the investigation are shown in Figure 1. Fixed contents (1 wt.%) of graphene and varying contents of MXene (0.5, 1, 1.5, and 2 wt.%) were mixed with nickel powder via a planetary ball milling machine (PM200, Ritsch Germany) for 4 hours with a ball milling speed of 250 rpm. Table 1 presents the composition and sample nomenclature of the different nickel-based composites reinforced with graphene (1 wt.%) and varying contents of $Ti_3C_2T_x$-MXene. The mass ratio of the ball to powder was kept at 10:1, and 1 wt.% citric acid was added to each composition as a process-controlling agent. After mixing, the blended powders were compacted by uniaxial cold pressing to form green pellets using a die steel mold with a 25 mm diameter at a pressure of 1.2 GPa. Afterwards, the obtained green pellets were sintered using a tube furnace at 1250 ˚C in a nitrogen atmosphere. The furnace was programmed to heat from room temperature to 1250 ˚C at 5 ˚C/min, soaking at 1250 ˚C for 2 hours, and then cooling in the furnace. Figure 2(a) and (b) present the schematic illustration of the complete procedure followed to synthesize Nickel-Graphene-MXene hybrid composites, along with the temperature-time diagram used for sintering. To ensure reproducibility, three independent samples were prepared for each composite composition following identical powder metallurgy processing conditions.

Characterization of Synthesized Nickel-Graphene-MXene Hybrid Composites

After cooling, the sintered composites were polished to achieve a surface finish of 0.2 µm using 800, 1000, 1200, 1500, and 2000 grit sandpaper and diamond paste, followed by ultrasonic cleaning with acetone and ethanol. The densities of the sintered composites were determined using Archimedes' principle. The microhardness of sintered composites was measured according to ASTM E92-23 standard [31] using a Micro-Vickers hardness testing machine (HM-200, Mitutoyo, India). The indenter was pressed into the specimen at a 1 kg load, which was maintained for a duration of 10 seconds.

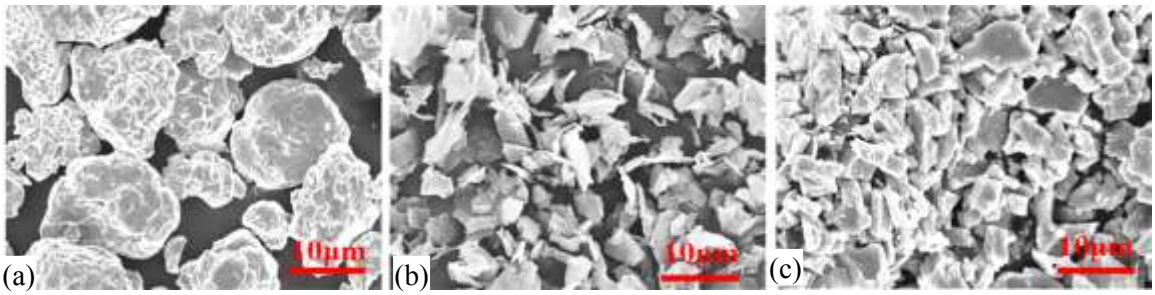

Figure 1. FESEM images of the powders used in the investigation: (a) pure Nickel, (b) Graphene, and (c) MXene.

© STM Journals 2025. All Rights Reserved

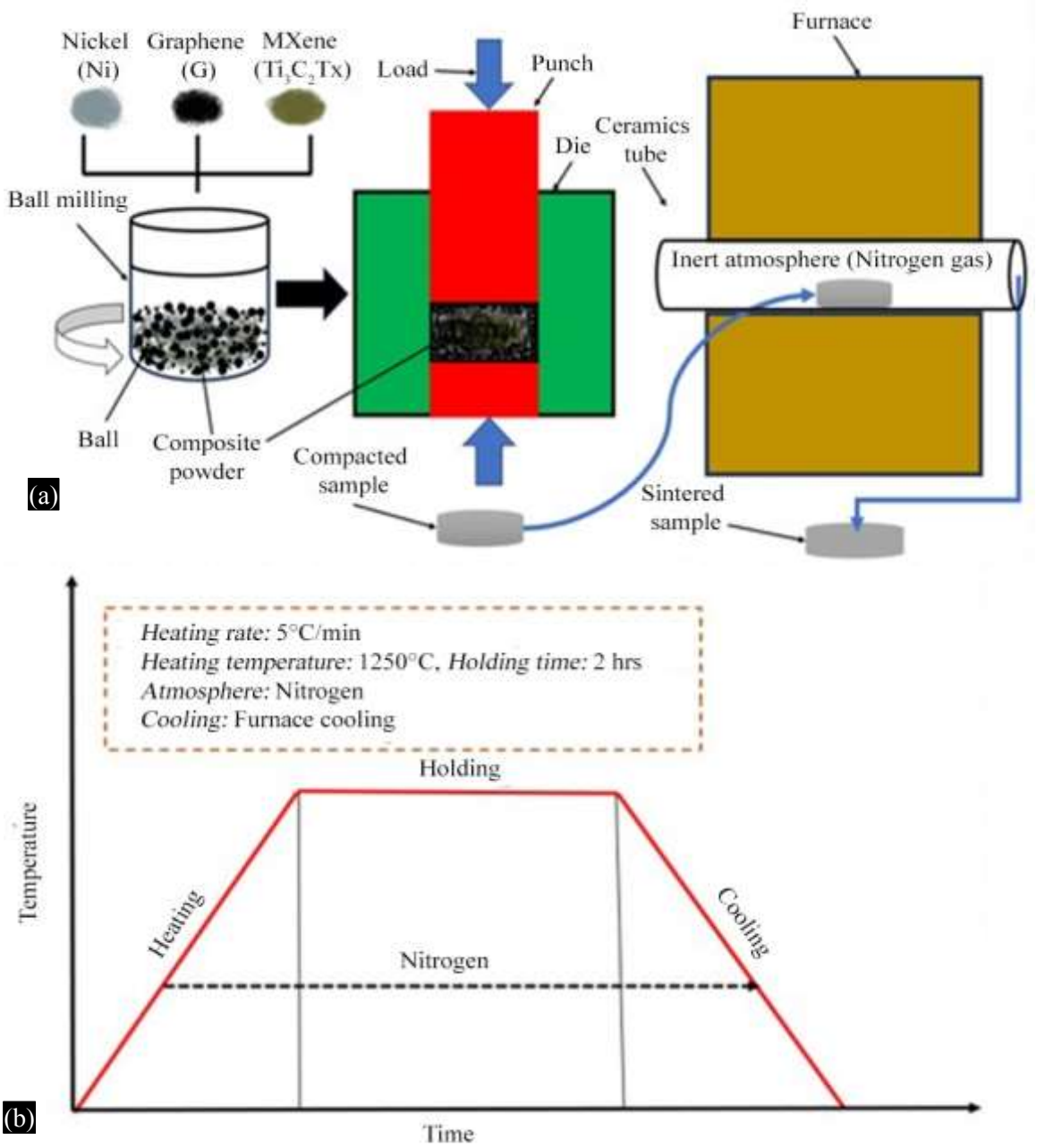

Figure 2. (a) Schematic diagram of the complete procedure followed to synthesize Nickel-Graphene-MXene composites, (b) Temperature-Time cycle used for sintering.

Six readings were taken on the surface of each composite, and the average hardness value was reported. The phases formed in the sintered composites were characterised by X-ray diffraction (D-8, Discover, Bruker Corp., Germany) using a step size of 0.02˚ over a scanning range of 5˚-80˚. Fourier-transform infrared spectroscopy (FTIR, Nicolet™ iS20, Thermo, USA) was used to characterize the functional groups on the surface before and after the sintering of Nickel-Graphene-MXene hybrid composites. The Raman spectroscopy (Lab RAM HRJovin Yvon) was used for further characterization of the Nickel-MXene-Graphene composites. The microstructure and surface morphology of the samples were observed using a field emission scanning electron microscope (FE-SEM JEOL, USA) and energy-dispersive spectroscopy (EDS).

Tribological Assessment of Nickel-Graphene-MXene Hybrid Composites

© STM Journals 2025. All Rights Reserved

The tribological properties of the fabricated composites were assessed in accordance with ASTM G99-23 [32] through a rotary ball-on-disk tribometer (TL-20, DUCOM, India). The sintered composites were rotated against a stationary silicon nitride (Si_3N_4) ball with a diameter of 6 mm, at a sliding speed of 0.25 m/s under a load of 10 N. The friction coefficient was recorded for a sliding distance of 500 m. The volumetric wear loss (V, mm^3) was measured using a 3D profilometer. The specific wear rate (W□) was then calculated using the relation: W□ = V / (L·S), where W□, V, L, and S represent the specific wear rate, volumetric loss, applied normal load, and sliding distance, respectively. After the tribological tests, the worn surfaces of the composites and counter balls were further analyzed using a 2D optical profilometer (DektakXT, Bruker, UK), X-ray diffraction (XRD), Raman spectroscopy, and FESEM equipped with energy-dispersive spectroscopy (EDS) to explore the underlying wear mechanisms.

RESULTS AND DISCUSSION

Characterization of Raw Materials and Blended Powders

Fourier Transform Infrared (FTIR) spectroscopy was employed to identify the functional groups present in the individual and blended powders, as displayed in Figure 3. In Figure 3(a), the FTIR spectrum of pure nickel exhibits characteristic peaks at 3861 cm^{-1}, 3696 cm^{-1}, 2326 cm^{-1}, 2117 cm^{-1}, 1685 cm^{-1}, and 1520 cm^{-1}, corresponding to functional groups such as O-H, O-H, C=O, Ni-C, C=O, and C-H. These vibrational modes indicate interactions between the nickel surface and hydroxyl groups, carbon-based species, and adsorbed atmospheric gases, suggesting its catalytic activity and surface reactivity. The FTIR spectrum of graphene, presented in Figure 3(b), reveals absorption bands

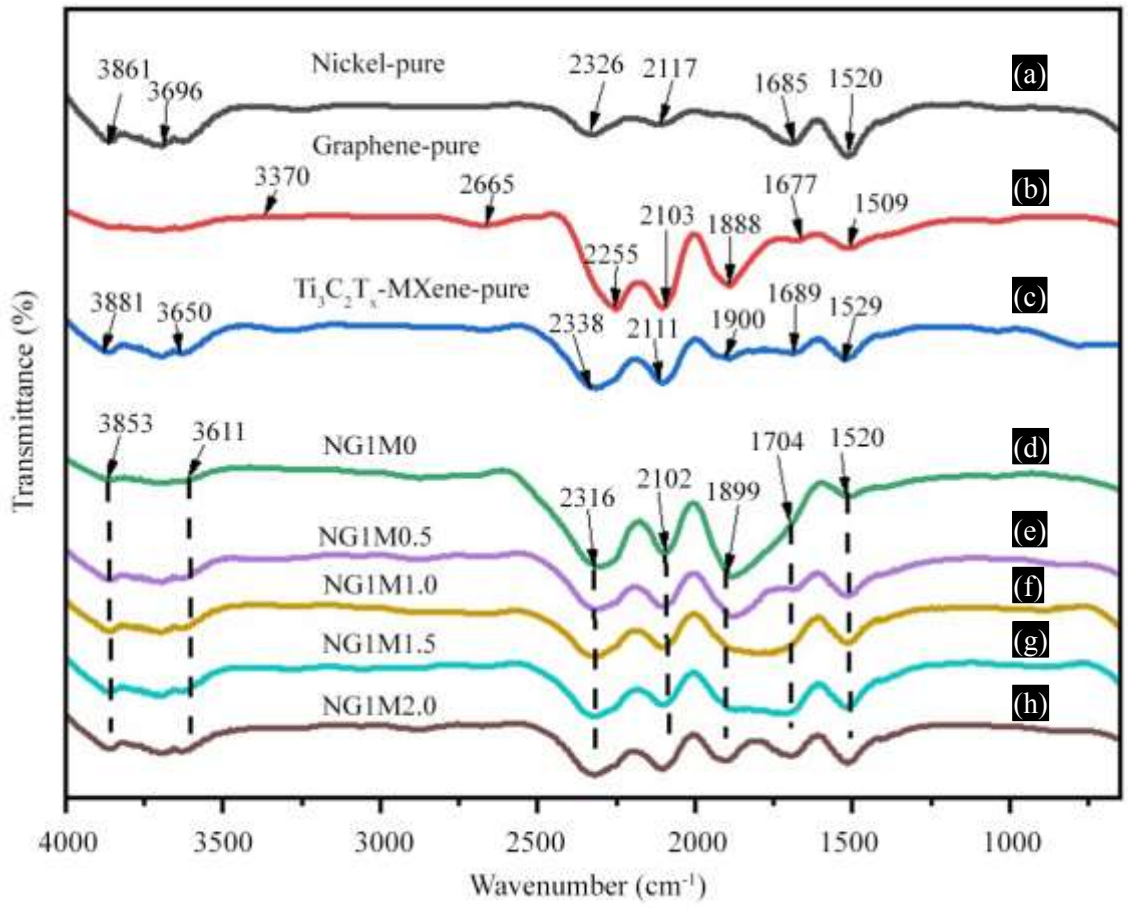

Figure 3. FTIR spectrum of powders (a) Nickel (b) Graphene (c) $Ti_3C_2T_x$-MXene (d) NG1M0 (e) NG1M0.5 (f) NG1M1.0 (g) NG1M1.5 (h) NG1M2.0.

© STM Journals 2025. All Rights Reserved

at 3370 cm^{-1}, 2665 cm^{-1}, 2255 cm^{-1}, 2103 cm^{-1}, 1888 cm^{-1}, 1677 cm^{-1}, and 1509 cm^{-1}. These peaks are attributed to O-H, O-H, C=O, C≡C, C=O, C-C, and C=C stretching vibrations, suggesting the presence of hydroxyl and carbonyl groups, adsorbed water and CO_2, and aromatic carbon structures on the graphene surface. The FTIR spectrum of $Ti_3C_2T_x$-MXene in Figure 3(c) shows absorption peaks at 3881 cm^{-1}, 3600 cm^{-1}, 2338 cm^{-1}, 2111 cm^{-1}, 1900 cm^{-1}, 1689 cm^{-1}, and 1529 cm^{-1}, which represent O-H, O-H, C=O, Ti-C, C=C, C=O, and C-H functionalities, confirming the presence of hydroxyl groups, surface oxides, and carbonaceous species, which are characteristic of the MXene surface termination groups. In the FTIR spectra of Nickel-Graphene-MXene composite powders, shown in Figure 3(d)–(h), prominent peaks appear at 3853 cm^{-1}, 3611 cm^{-1}, 2316 cm^{-1}, 2102 cm^{-1}, 1899 cm^{-1}, 1704 cm^{-1}, and 1520 cm^{-1}. These can be resemble with O-H, O-H, C=O, M-C, C=C, C=O, and C-C stretching vibrations, indicating the coexistence of hydroxyl groups, carbon-based species, and metal-carbon bonding. The presence of these functional groups highlights the successful integration and interaction of Graphene and MXene within the nickel matrix.

Figure 4 presents the Raman spectra of pure nickel, graphene, and MXene nanoparticles. As shown in Figure 4(a), pure nickel, being metallic in nature, exhibits no prominent Raman-active modes due to the lack of vibrational resonance with incident photons. However, weak and broad spectral features may occasionally appear due to surface roughening, which induces plasmonic effects or surface-enhanced Raman scattering. In contrast, the Raman spectrum of graphene, displayed in Figure 4(b), reveals the characteristic D and G bands at 1344 cm^{-1} and 1564 cm^{-1}, respectively. The G band arises from the phonon mode associated with in-plane sp^2 hybridized carbon vibrations, indicating an ordered hexagonal carbon lattice. The D band, on the other hand, is attributed to defect-induced breathing modes of aromatic rings, reflecting structural imperfections or functionalization. The intensity ratio of the D to G peaks (I_D/I_G) serves as a reliable indicator of the defect density and oxidation level within the graphene structure. Figure 4(c) shows the Raman spectrum of MXene ($Ti_3C_2T_x$), characterized by peaks at 266 cm^{-1}, 401 cm^{-1}, and 614 cm^{-1}. The 266 cm^{-1} band corresponds to out-of-plane vibrational modes, while the 401 cm^{-1} peak arises from in-plane lattice vibrations. The prominent 614 cm^{-1} peak is associated with Ti-C stretching vibrations, which are indicative of the layered carbide structure and the interaction between titanium and carbon atoms.

Figure 5 demonstrates the X-ray diffraction (XRD) patterns of pure nickel, graphene, and MXene nano powders, providing structural insights into their crystallographic phases and lattice arrangements. In Figure 5(a), the XRD pattern of pure nickel exhibits prominent diffraction peaks at 44.5° (111), 51.86° (200), and 76.39° (220), which are characteristic of a face-centered cubic (FCC) crystal structure (JCPDS Card No. 04-0850). Among these, the (111) plane shows the highest intensity, indicating it is the preferred orientation due to its high atomic packing density. Figure 5(b) displays the XRD spectrum of graphene nano powder, showing well-defined peaks at 26.48° (002) and 54.64° (004). The (002) reflection corresponds to the interlayer spacing between graphene sheets, typically associated with stacked graphene or few-layer graphene, while the (004) peak confirms the high crystallinity of the carbon structure. Figure 5(c) illustrates the XRD pattern of $Ti_3C_2T_x$-MXene, revealing multiple peaks at 8.36° (002), 35.92° (111), 41.72° (200), 60.52° (220), 72.44° (311), and 76.24° (222). The broad and intense (002) peak at low 2θ is a hallmark of MXene's lamellar structure, indicating expanded interlayer spacing caused by surface terminations (-OH, -O, -F) or intercalated species. The presence of higher-order peaks suggests a partially crystalline structure with retained order in the layered MXene framework. In summary, the XRD analysis confirms that nickel exhibits a well-defined FCC structure, graphene maintains high crystallinity, and MXene retains its distinctive layered configuration, each contributing structurally unique characteristics essential for composite formation and potential synergistic performance in tribological applications. Figure 6 depicts the X-ray diffraction (XRD) peaks of blended Nickel-Graphene-MXene nanocomposite powders, highlighting the structural properties and interactions of the constituent components. The peaks for MXene (002), Graphene (002), and Nickel (111), (200), and (220) provide valuable information

© STM Journals 2025. All Rights Reserved

regarding the crystallinity and phase composition of the composite. The (002) peak of MXene ($Ti_3C_2T_x$)

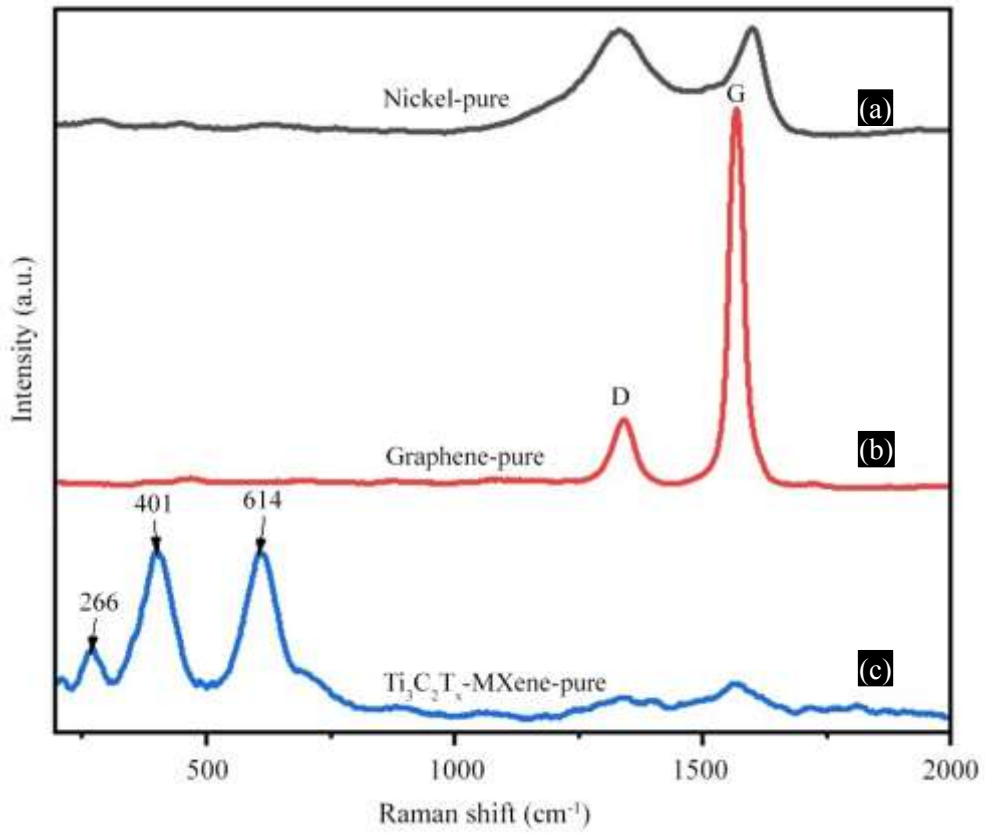

Figure 4. Raman spectra of (a) pure Nickel, (b) Graphene, (c) MXene nano-powders.

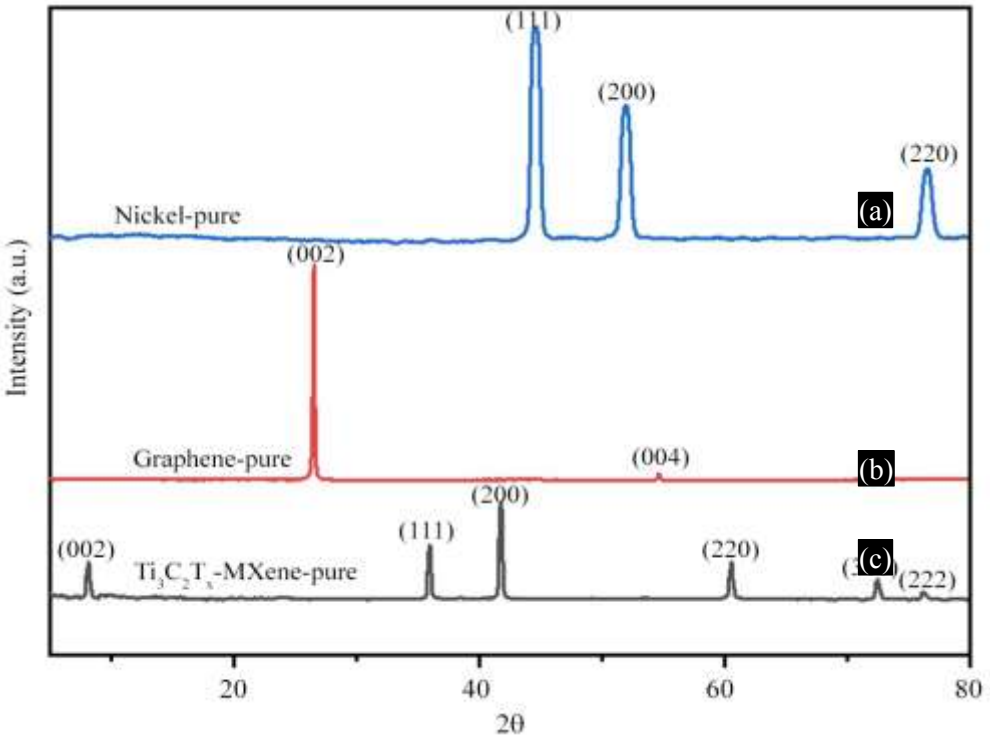

Figure 5. XRD patterns of raw materials (a) Pure Nickel, (b) Graphene, (c) MXene nano powders.

© STM Journals 2025. All Rights Reserved

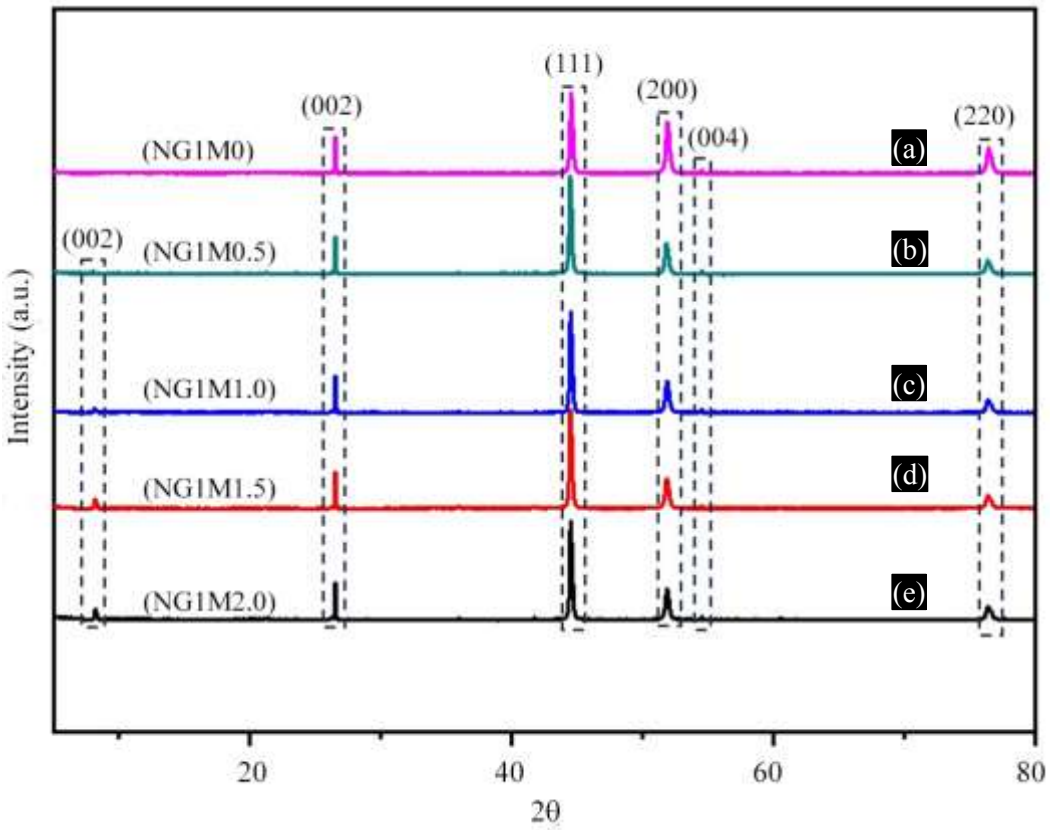

Figure 6. XRD patterns of (a) NG1M0, (b) NG1M0.5, (c) NG1M1.0, (d) NG1M1.5, (e) NG1M2.0 nano composite powders after ball milling.

reflects interlayer spacing, while the graphene peaks, often about 26.48° 2θ, indicate graphene stacking. The XRD analysis demonstrates that the nanocomposite was successfully produced with the right phase composition. However, the emergence of these peaks indicates that the material is going through phase separation or aggregation, which might have a negative impact on its performance.

Figure 7 highlights the significance of FESEM imaging and EDX analysis in characterizing the morphological and compositional features of Nickel-Graphene-MXene nanocomposite powders. Figure 7(a) shows the microstructure of pure nickel nanoparticles after ball milling, displaying uniform particle distribution. Figures 7(b) and (c) correspond to Nickel-1 wt.% Graphene and Nickel-1 wt.% Graphene- 0.5 wt.% MXene blended powders, respectively, revealing the impact of individual additives on particle morphology. Figure 7(d) presents the Nickel-1 wt.% Graphene with 1 wt.% MXene composite, while Figure 7(e) and (f) demonstrate Nickel-1 wt.% Graphene with 1.5 wt.% and 2.0 wt.% MXene, respectively. These micrographs collectively demonstrate the influence of varying MXene content on the microstructural evolution of the composite powder along with elemental distribution. These methods provide valuable information on the nanocomposites' structure, elemental composition, and dispersion. FESEM imaging combined with EDX analysis gives a full understanding of nanocomposites, which aids in the optimization of manufacturing processes and performance for a wide range of applications. The ball milling process has a significant influence on the nanocomposites' structure by reducing particle size and increasing component dispersion. It enhances material performance by dispersing nickel nanoparticles, exfoliating MXene sheets, and evenly scattering graphene. This homogeneous mixing and dispersion may lead to improved composite properties. Furthermore, the EDX spectrum shows a consistent distribution of nickel, carbon, titanium, and oxygen throughout the nanocomposite powders. This investigation contributes to a better understanding of nanocomposites' composition and performance.

© STM Journals 2025. All Rights Reserved

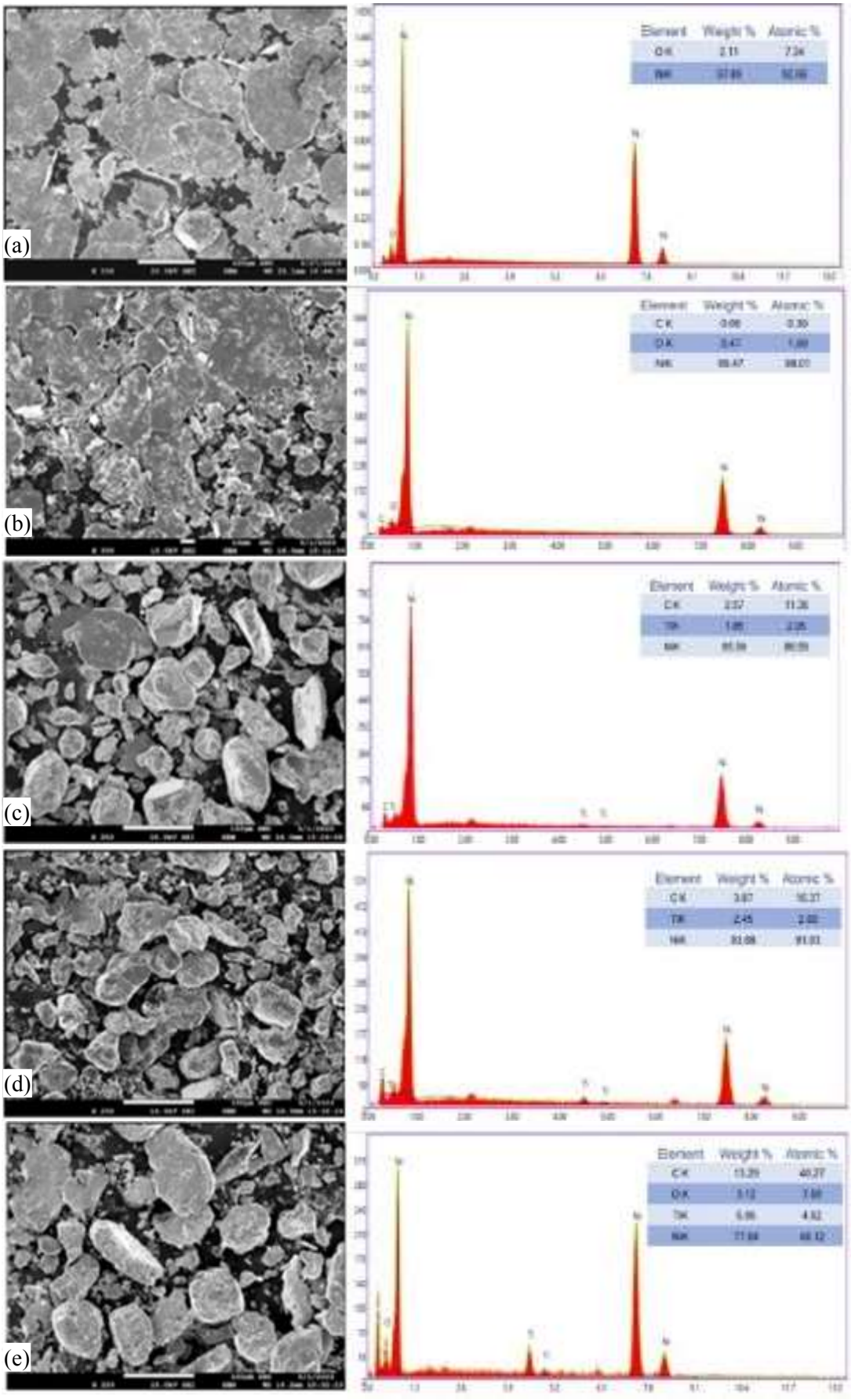

© STM Journals 2025. All Rights Reserved

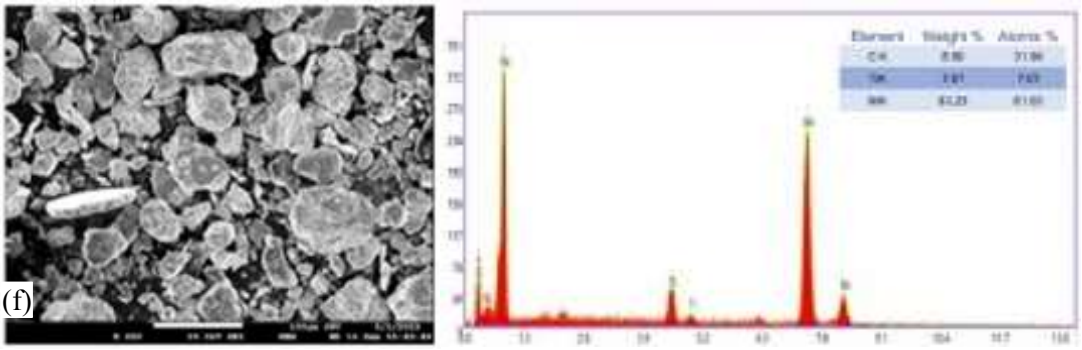

Figure 7. FESEM and EDX morphologies of (a) NG1M0, (b) NG1M0.5, (c) NG1M1.0, (d) NG1M1.5, (e) NG1M2.0 nano composite powders after ball milling.

Table 1. Composition, sample nomenclature, microhardness, and density of the sintered composites.

Composition (wt.%)			Sample nomenclature	Microhardness (HV)	Density (gm/cm^3)
Nickel	*Graphene*	*$Ti_3C_2T_x$-MXene*			
100	-	-	NG0M0	108 ± 5	8.51 ± 0.17
99	1	-	NG1M0	114 ± 4	8.28 ± 0.11
98.5	1	0.5	NG1M0.5	125 ± 3	8.07 ± 0.15
98	1	1.0	NG1M1.0	138 ± 3	8.02 ± 0.09
97.5	1	1.5	NG1M1.5	147 ± 2	7.83 ± 0.13
97	1	2.0	NG1M2.0	157 ± 4	7.6 ± 0.07

Characterization of Sintered Nickel-Graphene-MXene Hybrid Composites

Table 1 displays the composition, sample nomenclature, microhardness, and density of the sintered nickel-based composites reinforced with graphene (1 wt.%) and varying contents of $Ti_3C_2T_x$-MXene. Pure nickel (NG0M0) exhibits a microhardness of 108 HV and a density of 8.51 g/cm³. With the addition of 1 wt.% graphene (NG1M0), the microhardness increases to 114 HV, accompanied by a slight decrease in density to 8.28 g/cm³, indicating the strengthening effect of graphene. A progressive increase in MXene content, from 0.5 wt.% to 2 wt.% (samples NG1M0.5 to NG1M2.0), leads to a consistent enhancement in microhardness, reaching 157 HV for the highest MXene loading. Concurrently, the average density decreases from 8.07 g/cm³ (NG1M0.5) to 7.60 g/cm³ (NG1M2.0), likely due to the lower intrinsic density of MXene compared to nickel. These results demonstrate a synergistic improvement in hardness through the combined addition of graphene and MXene, though at the expense of a gradual reduction in composite density. One can conclude that the NG1M2.0 composite has revealed approximately a 45.4% increase in average hardness and a 10.7% decrease in average density compared to pure nickel, i.e., NG0M0. The relatively narrow error margins (± 2–5 HV for hardness and ± 0.07–0.17 g/cm³ for density) confirm good repeatability.

Figure 8 presents the X-ray diffraction (XRD) analysis of sintered composite samples. Figure 8(a) displays the XRD pattern of pure nickel, with distinct peaks at 2θ values of 43.94°, 51.21°, and 75.90°, corresponding to the (111), (200), and (220) crystallographic planes of the face-centered cubic (FCC) structure. The sharpness and intensity of these peaks confirm the high crystallinity and phase purity of the nickel sample. Figure 8(b) shows the XRD pattern of the Nickel-Graphene sintered composite. Peaks observed at 26.03°, 44.55°, 51.82°, 54.71°, and 76.41° indicate the successful integration of graphene within the nickel matrix. The peak near 26.03° corresponds to the (002) plane of graphene, while the remaining peaks are associated with the FCC structure of nickel, suggesting a well-dispersed graphene phase in the composite. Figures 8(c)–(f) reveal the XRD patterns of the Nickel-Graphene-MXene composites with varying MXene content. The observed peaks at 8.82°, 26.24°, 43.96°, 51.31°, 54.80°, and 75.90° correspond to the (002) plane of MXene, the (002) plane of graphene, and the (111), (200), (004), and (220) planes of nickel, respectively. The emergence of the MXene (002) peak at 8.82°

© STM Journals 2025. All Rights Reserved

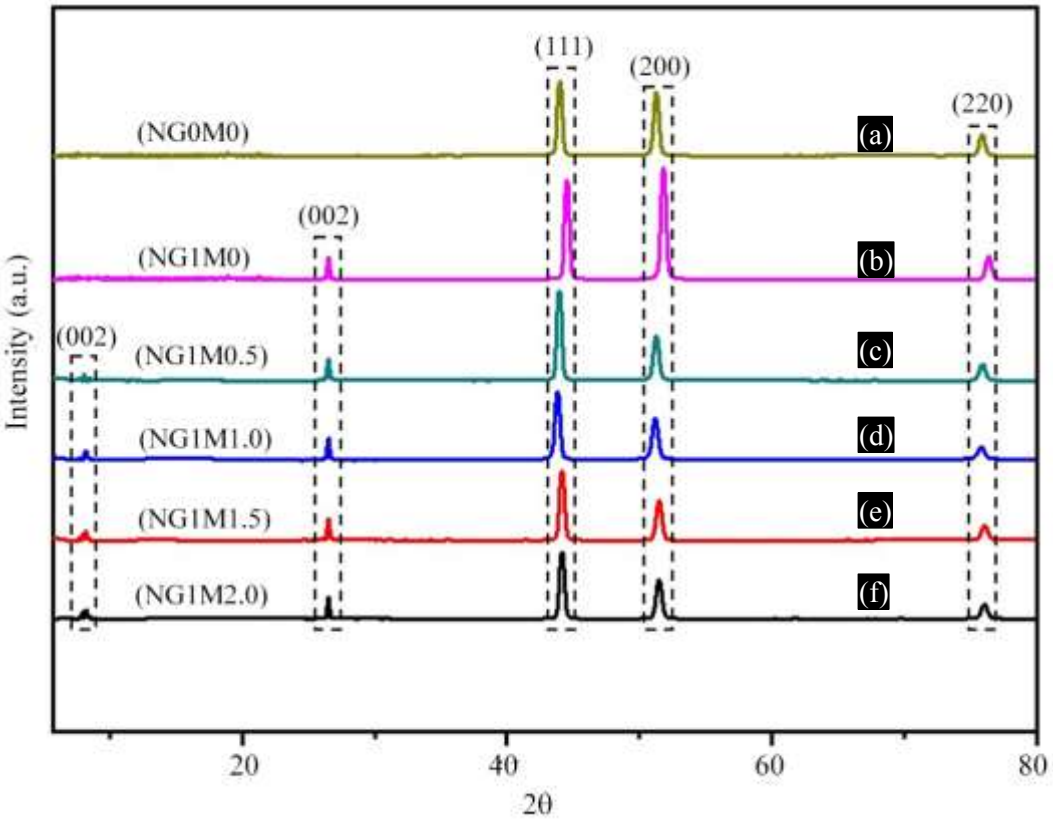

Figure 8. The XRD patterns of the Nickel-Graphene-MXene compacted sintered composite samples.

confirms the incorporation of layered $Ti_3C_2T_x$ structures into the composite. The coexistence of diffraction peaks from nickel, graphene, and MXene indicates the formation of a multiphase composite system. Overall, the XRD results confirm the successful synthesis of structurally integrated Nickel-Graphene-MXene composites with well-defined crystalline phases. The increased complexity of the diffraction patterns with the addition of graphene and MXene reflects the evolving structural arrangement and phase interactions within the sintered composite materials.

Tribological Assessment of Nickel-Graphene-MXene Hybrid Composites

Figure 9 shows the trends of friction coefficient with time for sintered samples NG0M0, NG1M0, NG1M0.5, NG1M1.0, NG1M1.5, and NG1M2.0 tested under identical tribological testing conditions, i.e., a load of 10 N and a sliding velocity of 0.25 m/s. The curve, corresponding to the pure nickel sample (NG0M0), exhibits the highest and most unstable friction coefficient, fluctuating significantly around ~0.79 throughout the test duration. This behavior indicates poor wear resistance and the absence of any solid lubricant phase in the matrix, leading to high interfacial shear and surface damage. In contrast, the addition of 1 wt.% graphene (NMG1M0) results in a notable reduction in the friction coefficient to around 0.42, with improved stability. This reduction is attributed to the lubricating nature of graphene, which forms a tribo-layer at the contact interface and reduces direct metal-to-metal contact. Further enhancements are observed as MXene is incrementally introduced into the composite. Samples NG1M0.5, NG1M1.0, and NG1M1.5 show a progressively decreasing and more stable friction coefficient, stabilizing in the range of 0.35-0.39. The most significant improvement is observed for NG1M2.0 with an average COF ~ 0.31. This trend highlights the synergistic effect of graphene and MXene in improving the tribological performance of composite. The MXene's layered structure, combined with its high mechanical strength and surface activity, contributes to reduced friction by promoting easy shear and wear debris entrapment.

© STM Journals 2025. All Rights Reserved

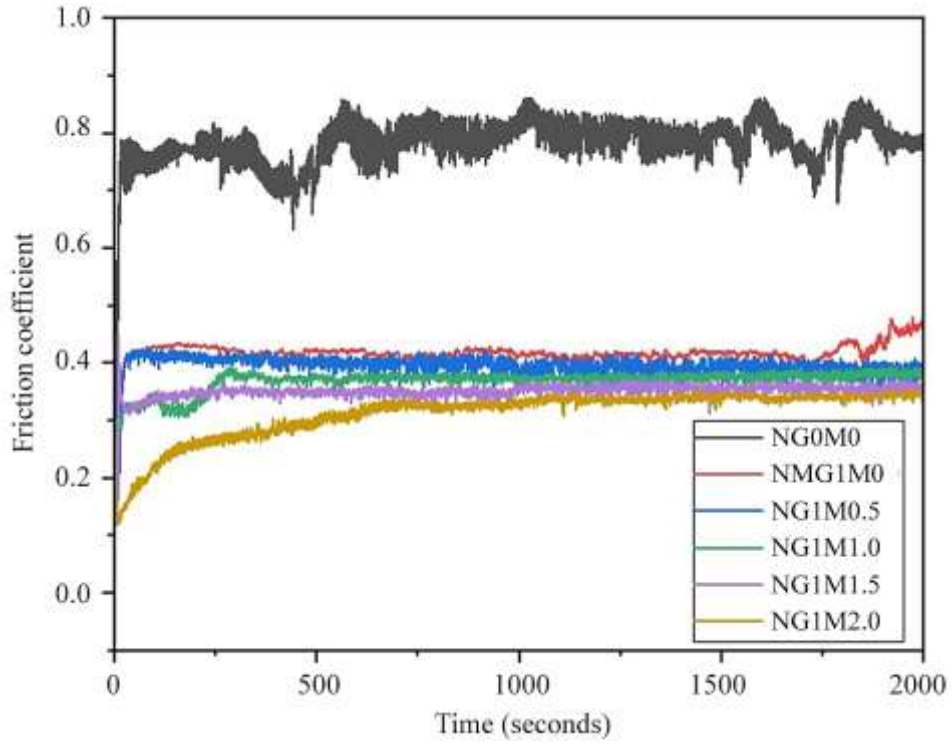

Figure 9. Variation in friction curve with time for NG0M0, NG1M0, NG1M0.5, NG1M1.0, NG1M1.5, and NG1M2.0.

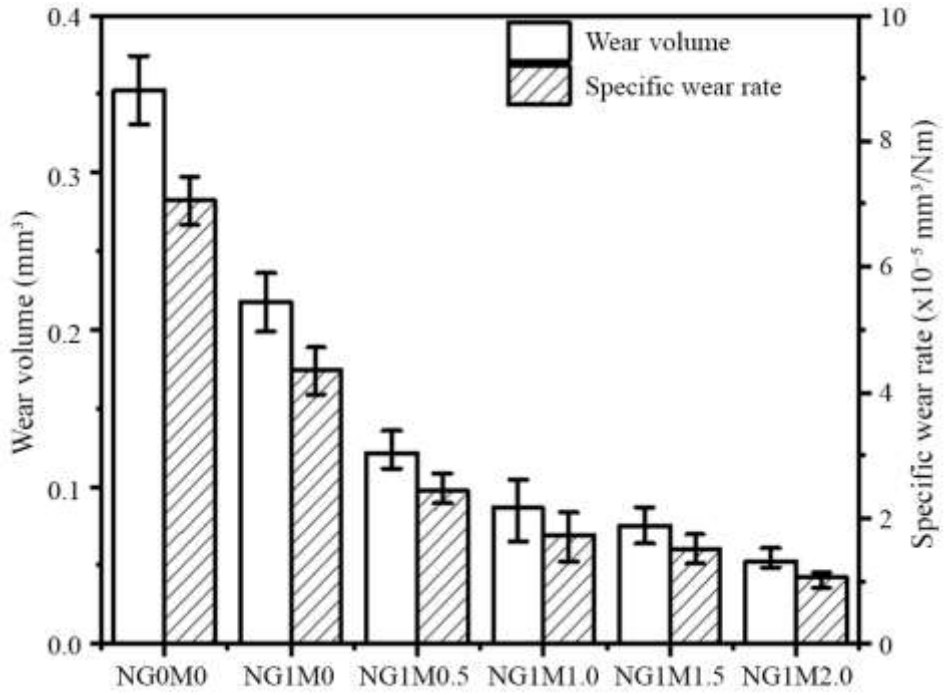

Figure 10. Wear volume and specific wear rate for NG0M0, NG1M0, NG1M0.5, NG1M1.0, NG1M1.5, and NG1M2.0.

Figure 10 illustrates the wear performance of sintered Nickel-Graphene-MXene nanocomposite samples in terms of wear volume and specific wear rate. The graph demonstrates the progressive improvement in wear resistance as graphene and MXene contents are systematically introduced into

© STM Journals 2025. All Rights Reserved

the nickel matrix. The pure nickel sample (NG0M0) exhibits the highest wear volume (~0.35 mm³) and a specific wear rate approaching ~7.05×10^{-5} mm³/N·m, indicating poor wear resistance due to the absence of solid lubricants or reinforcements. Upon the addition of 1 wt.% graphene (NG1M0), a significant reduction in wear volume and wear rate is observed, confirming the beneficial role of graphene in reducing interfacial shear and enhancing load-carrying capacity. As MXene is progressively incorporated (from 0.5 to 2.0 wt.%), both wear volume and specific wear rate continue to decline across the samples NG1M0.5, NG1M1.0, NG1M1.5, and NG1M2.0. The sample NG1M2.0 demonstrates the lowest wear volume (~0.05 mm³) and a specific wear rate below 1.05×10^{-5} mm³/N·m, reflecting the optimal synergistic interaction between graphene and MXene within the nickel matrix. This improvement is attributed to the combined effects of graphene's excellent lubrication and MXene's high hardness and layered structure, which together form a stable and protective tribo-layer during sliding. The decreasing trend in both metrics confirms that reinforcement with graphene and MXene significantly enhances the wear resistance of nickel-based composites by reducing material removal and improving load distribution under tribological loading. These findings emphasize the potential of Nickel-Graphene-MXene composites for applications requiring high durability and low wear under sliding contact.

Analysis of Worn Surfaces

The worn surface morphology and corresponding elemental composition of the sintered composites were investigated using FESEM and EDS, as shown in Figure 11. The pure Nickel sample (NG0M0) displayed a severely damaged surface characterized by large grooves and delamination features, indicative of dominant adhesive wear. With the incorporation of 1 wt% graphene (NG1M0), a noticeable reduction in surface damage was observed, with smoother grooves suggesting improved load-bearing capacity and lubricity due to graphene reinforcement. Further addition of MXene (samples NG1M0.5 to NG1M2.0) led to progressive refinement in surface morphology. The NG1M0.5 and NG1M1.0 samples showed fewer grooves and more uniform wear patterns, while the NG1M1.5 and NG1M2.0 composites exhibited smoother surfaces with finely distributed wear debris, indicative of enhanced tribological stability and reduced material removal. The EDS spectra confirmed the presence of carbon and oxygen from graphene and surface oxidation, respectively, while titanium and silicon peaks confirmed the successful integration of MXene. A steady increase in carbon and titanium content, particularly in NG1M2.0, correlated with the improved surface characteristics. The highest carbon (8.94 wt%) and titanium (3.48 wt%) contents were recorded in NG1M2.0, which also displayed the smoothest worn surface, indicating optimal reinforcement distribution and synergistic wear resistance provided by graphene and MXene. Overall, the combined effect of graphene and MXene significantly contributed to improved wear performance, with NG1M2.0 exhibiting the most favourable tribological behavior among the tested compositions.

Figure 12 illustrates the FESEM micrograph of the worn scar on a silicon nitride (Si_3N_4) ball after sliding against the NG1M2.0 composite, along with the corresponding EDS spectra for selected regions. The worn surface (Figure 12(a)) shows a well-developed transfer layer with distinct grooves aligned along the sliding direction, indicative of consistent sliding contact and formation of a tribo-layer. Three regions (Area 1, Area 2, and Area 3) were analyzed via EDS to identify the compositional nature of the transferred material. The EDS spectra (Figure 12(b)–(d)) from all three areas reveal significant peaks corresponding to C, O, Si, Ti, and Ni. The presence of nickel and titanium signals across all regions confirms the transfer of metallic constituents from the NG1M2.0 composite onto the Si_3N_4 counter-face, suggesting material adhesion and tribo-layer formation during sliding. The strong silicon peaks are attributed to the Si_3N_4 substrate, while the appearance of carbon and oxygen indicates the participation of graphene and possible surface oxidation. The detection of titanium further validates the active role of MXene in forming the tribo-layer, which likely contributes to observed enhancement in wear resistance and frictional behavior. The uniform distribution of

© STM Journals 2025. All Rights Reserved

transferred elements across all analyzed areas highlights the stability and effectiveness of the protective layer formed during tribological interaction with the NG1M2.0 composite.

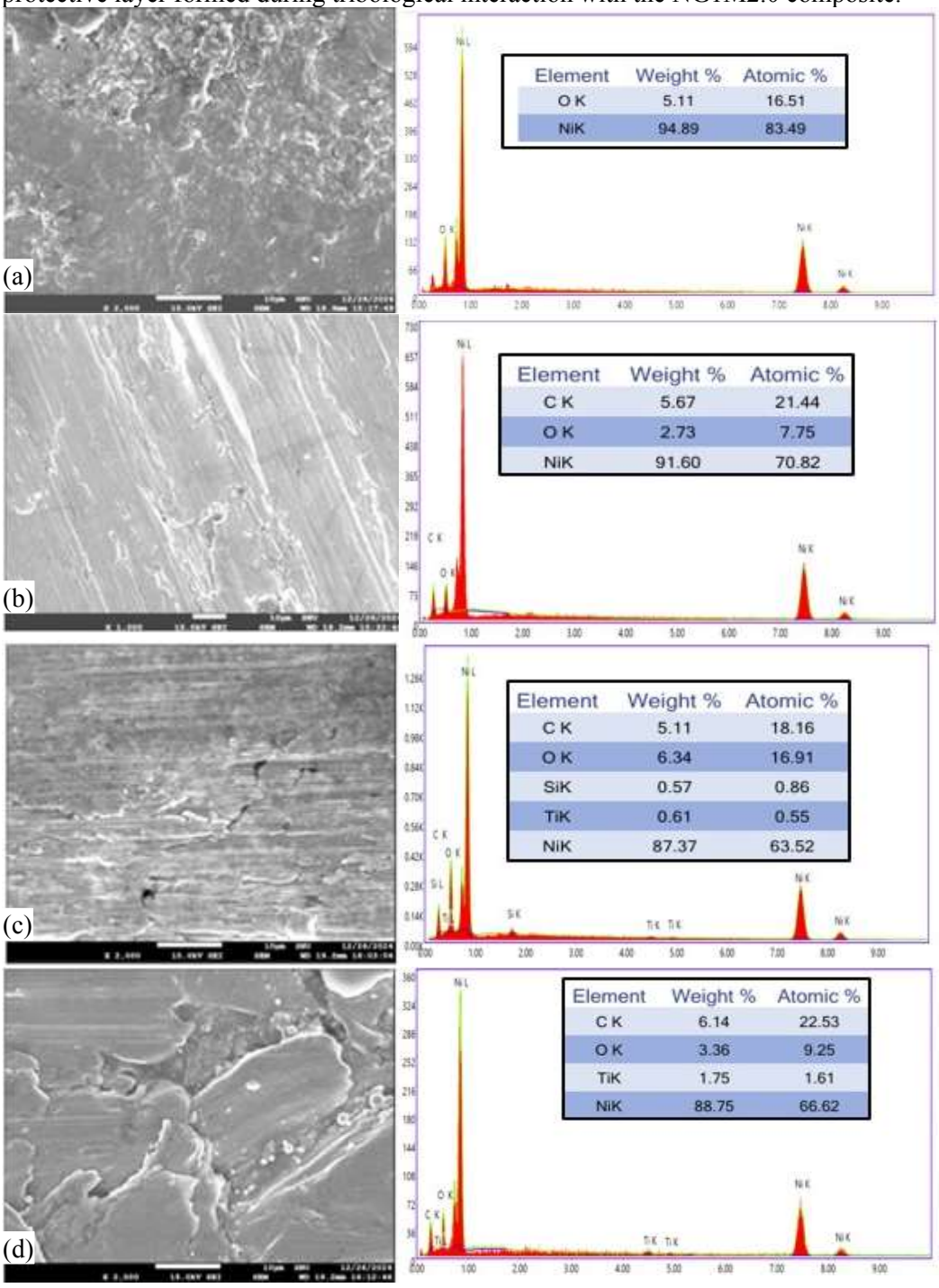

© STM Journals 2025. All Rights Reserved

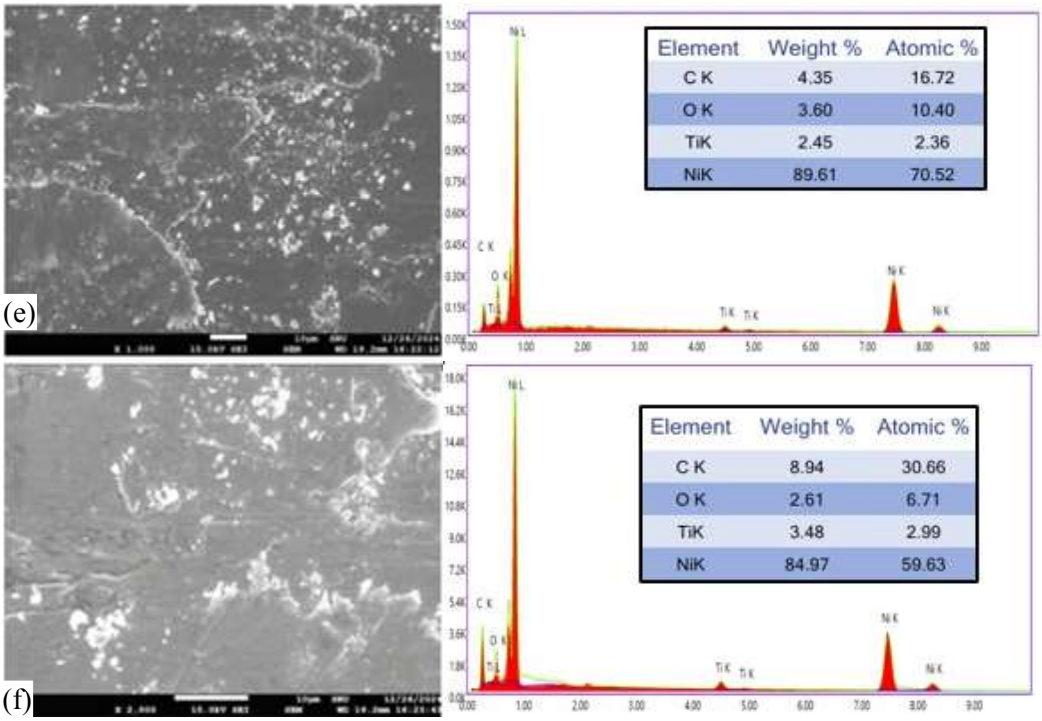

Figure 11. FESEM and EDS morphologies of worn surfaces of (a) NG0M0, (b) NG1M0, (c) NG1M0.5, (d) NG1M1.0, (e) NG1M1.5, (f) NG1M2.0.

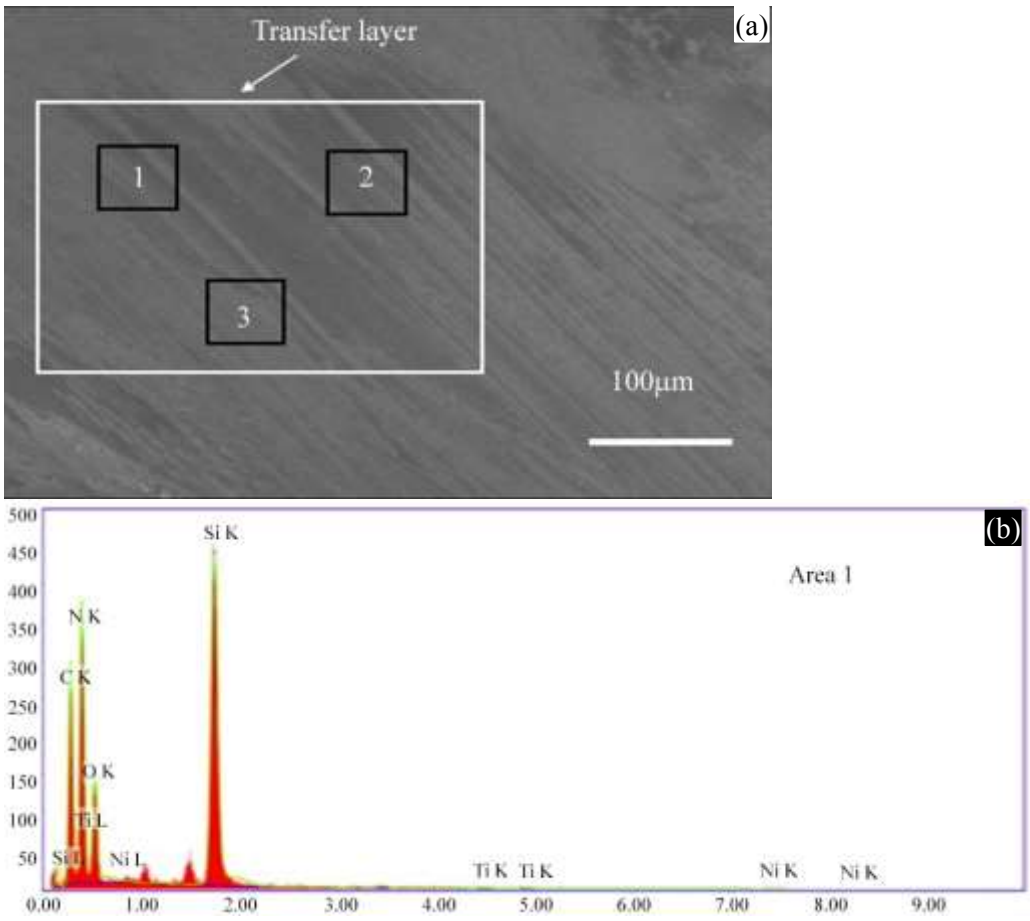

© STM Journals 2025. All Rights Reserved

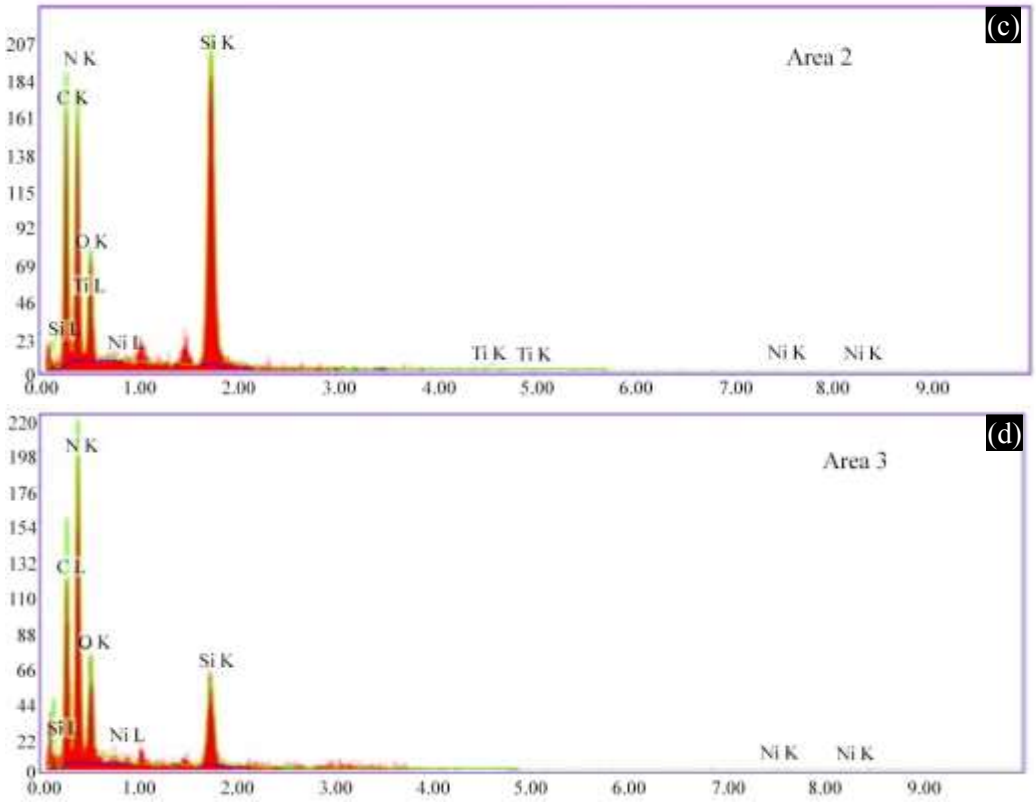

Figure 12. FESEM morphology of Si_3N_4 ball worn scar and EDS spectrum of the marked areas of silicon nitride ball slid against NG1M2.0 composites.

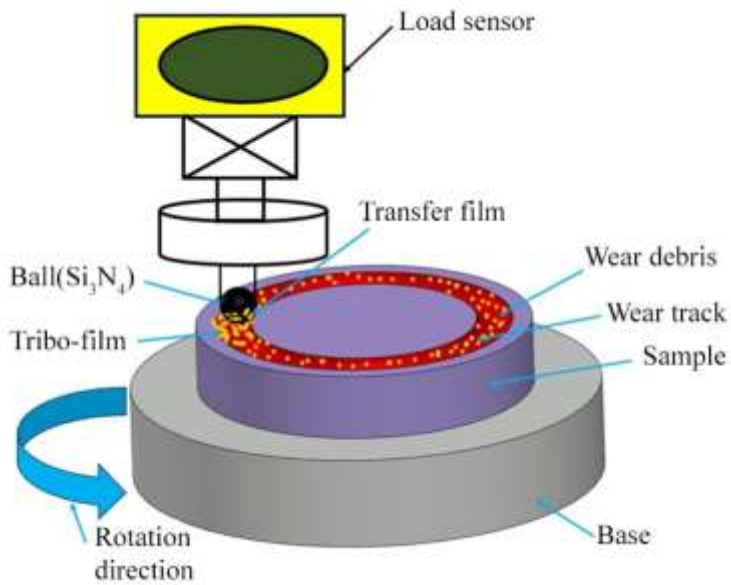

Figure 13. Schematic diagram of the possible wear Mechanism involved in the friction test.

Figure 13 demonstrates a schematic representation of a possible wear mechanism occurring during the ball-on-disk tribological test using a Si_3N_4 ball against the composite sample. A tribo-film develops on wear track of the sample surface due to mechanical interaction and chemical reactions at the sliding interface. Concurrently, a transfer film of Ni, Si, Ti, C, and O elements forms on the counter-face (Si_3N_4 ball) as fragments of the composite material adhere to it, enhancing lubrication

© STM Journals 2025. All Rights Reserved

and reducing direct asperity contact. The tribo-film and transfer film play a crucial role in stabilizing friction and minimizing wear by acting as protective layers that reduce metal-to-metal contact. The formation of these films indicates a complex combination of adhesive, abrasive, and tribo-chemical wear mechanisms, wherein the synergistic effect of the reinforcing phases (e.g., MXene and graphene) contributes to improved wear resistance by enhancing film stability and integrity under repeated sliding cycles.

The present results demonstrate that the incorporation of 1 wt.% graphene and 2 wt.% MXene into a nickel matrix yields a ~45.4% increase in microhardness, a ~60.7% reduction in friction coefficient, and an ~85.1% decrease in wear rate relative to pure nickel. These improvements compare favorably with earlier reports on nickel- or Ni_3Al-based composites reinforced with 2D materials. Yan et al. [28] observed significant friction and wear reduction in Ni_3Al-graphene-Ti_3SiC_2 composites, but the hardness improvement was comparatively modest (<20%). Similarly, Singh et al. [30] reported that $Ti_3C_2T_x$-MXene-reinforced Ni_3Al alloys could achieve remarkable tribological performance, though density penalties and processing complexity were more pronounced. Compared with polymer- and ceramic-based MXene composites [24,29], which showed improved tribological stability but limited hardness enhancement, the present Ni-Graphene-MXene system achieves a synergistic balance of mechanical strengthening and lubrication. Importantly, the combination of graphene and MXene provides dual reinforcement: graphene contributes to solid lubrication and load distribution, while MXene enhances hardness and supports stable tribo-film formation. This dual mechanism differentiates the current findings from single-additive systems and underlines the novelty of the hybrid approach for achieving simultaneously higher hardness and superior wear resistance.

CONCLUSION

In this study, novel Nickel-Graphene-MXene hybrid nanocomposites were successfully fabricated using a powder metallurgy approach and systematically evaluated for their tribological performance. The incorporation of 1 wt.% graphene and varying contents of $Ti_3C_2T_x$-MXene (0.5-2.0 wt.%) significantly enhanced the mechanical and tribological properties of the nickel matrix. The composite containing 2.0 wt.% MXene (NG1M2.0) exhibited the best performance, with a ~45% increase in microhardness and a ~10% reduction in density compared to pure nickel. The synergistic effect of graphene and MXene resulted in a substantial reduction in both the friction coefficient (from ~0.79 to ~0.31) and specific wear rate (from ~7.05×10^{-5} to <1.05×10^{-5} $mm^3/N \cdot m$), attributed to the formation of stable tribo- and transfer films. Surface characterization of the worn samples and Si_3N_4 counterface confirmed the presence of these protective films, which minimized adhesive and abrasive wear. The findings demonstrate that the combined addition of graphene and MXene not only enhances load-carrying capacity and lubrication but also promotes structural integrity during dry sliding. These composites are promising candidates for high-performance applications requiring superior wear resistance and mechanical reliability, particularly in aerospace and automotive sectors.

REFERENCES

1. Khan F, Hossain N, Mim JJ, Rahman SM, Iqbal MJ, Billah M, et al. Advances of composite materials in automobile applications – A review. J Eng Res. 2025;13:1001–23. https://doi.org/10.1016/j.jer.2024.02.017.
2. Sharma M, Babu DV, Gour M, Anandhan A, Kumar S, K JGL. Design and Characterization of High-Performance Polymer Nanocomposites for Aerospace Applications. J Polym Compos. 2025;13:178–93.
3. Nautiyal H, Singh S, Gautam RKS, Goswami RN, Khatri OP, Verma P, et al. The state of art on lubrication methods in space environment. Phys Scr. 2024;99. https://doi.org/10.1088/1402-4896/ad1d3e.
4. Gautam RKS, Tripathi VM, Gautam JK, Singhania S, Singh S, Jha P, et al. Elevated temperature tribological assessment of Ni-based cermet self-lubricating coatings deposited by cold spray. Surf Coatings Technol. 2024;477:130380. https://doi.org/10.1016/j.surfcoat.2024.130380.

© STM Journals 2025. All Rights Reserved

5. John M, Menezes PL. Self-lubricating materials for extreme condition applications. Materials (Basel). 2021;14:5588. https://doi.org/10.3390/ma14195588.
6. Holmberg K, Erdemir A. Influence of tribology on global energy consumption, costs and emissions. Friction. 2017;5:263–84. https://doi.org/10.1007/s40544-017-0183-5.
7. Erdemir A, Ramirez G, Eryilmaz OL, Narayanan B, Liao Y, Kamath G, et al. Carbon-based tribofilms from lubricating oils. Nature. 2016;536:67–71. https://doi.org/10.1038/nature18948.
8. Berman D, Deshmukh SA, Sankaranarayanan SKRS, Erdemir A, Sumant A V. Macroscale superlubricity enabled by graphene nanoscroll formation. Science. (80) 2015;348:1118–22. https://doi.org/10.1126/science.1262024.
9. Dwivedi N, Ott AK, Sasikumar K, Dou C, Yeo RJ, Narayanan B, et al. Graphene overcoats for ultra-high storage density magnetic media. Nat Commun. 2021;12:1–13. https://doi.org/10.1038/s41467-021-22687-y.
10. Dwivedi N, Neogi A, Patra TK, Dhand C, Dutta T, Yeo RJ, et al. Angstrom-Scale Transparent Overcoats: Interfacial Nitrogen-Driven Atomic Intermingling Promotes Lubricity and Surface Protection of Ultrathin Carbon. Nano Lett. 2021;21:8960–9. https://doi.org/10.1021/acs.nanolett.1c01997.
11. Bharti P, Sunkara SV, Vishwakarma J, Jaiswal S, Dhand C, Kumar R, et al. Simultaneous Control of Sliding Contact and Oxidation via Graphene-Based Materials. ACS Appl Eng Mater. 2023;1:2062–74. https://doi.org/10.1021/acsaenm.3c00222.
12. Lee C, Li Q, Kalb W, Liu XZ, Berger H, Carpick RW, et al. Frictional characteristics of atomically thin sheets. Science. (80) 2010;328:76–80. https://doi.org/10.1126/science.1184167.
13. Bharti P, Neogi A, Sharma R, Dhand C, Kumar R, Kumar P, et al. Decision trees within 1D/2D material systems for enabling highly lubricious and wear resistant surfaces. Carbon N Y. 2024;217:118603. https://doi.org/10.1016/j.carbon.2023.118603.
14. Mukhtar F, Munawar T, Nadeem MS, ur Rehman MN, Mahmood K, Batool S, et al. Enhancement in carrier separation of ZnO-Ho2O3-Sm2O3 hetrostuctured nanocomposite with rGO and PANI supported direct dual Z-scheme for antimicrobial inactivation and sunlight driven photocatalysis. Adv Powder Technol. 2021;32:3770–87. https://doi.org/10.1016/j.apt.2021.08.022.
15. Munawar T, Mukhtar F, Nadeem MS, Mahmood K, Hasan M, Hussain A, et al. Novel direct dual-Z-scheme ZnO-Er2O3-Nd2O3@reduced graphene oxide heterostructured nanocomposite: Synthesis, characterization and superior antibacterial and photocatalytic activity. Mater Chem Phys. 2020;253:123249. https://doi.org/10.1016/j.matchemphys.2020.123249.
16. Berman D, Erdemir A, Sumant A V. Graphene: A new emerging lubricant. Mater Today. 2014;17:31–42. https://doi.org/10.1016/j.mattod.2013.12.003.
17. Zeng X, Peng Y, Lang H. A novel approach to decrease friction of graphene. Carbon N Y. 2017;118:233–40. https://doi.org/10.1016/j.carbon.2017.03.042.
18. Patil SJ, Gawande GD, Khairnar Y, Sharma M, Patil MK. Graphene-Polymer Nanocomposites for Drug Delivery Applications. J Polym Compos. 2025;13:362–74.
19. Rosenkranz A, Liu Y, Yang L, Chen L. 2D nano-materials beyond graphene: from synthesis to tribological studies. vol. 10. Springer International Publishing; 2020. https://doi.org/10.1007/s13204-020-01466-z.
20. Berman D, Narayanan B, Cherukara MJ, Sankaranarayanan SKRS, Erdemir A, Zinovev A, et al. Operando tribochemical formation of onion-like-carbon leads to macroscale superlubricity. Nat Commun. 2018;9. https://doi.org/10.1038/s41467-018-03549-6.
21. Berman D, Erdemir A, Sumant A V. Approaches for Achieving Superlubricity in Two-Dimensional Materials. ACS Nano. 2018;12:2122–37. https://doi.org/10.1021/acsnano.7b09046.
22. Naguib M, Kurtoglu M, Presser V, Lu J, Niu J, Heon M, et al. Two-dimensional nanocrystals produced by exfoliation of Ti 3AlC 2. Adv Mater. 2011;23:4248–53. https://doi.org/10.1002/adma.201102306.
23. Naguib M, Mochalin VN, Barsoum MW, Gogotsi Y. 25th anniversary article: MXenes: A new family of two-dimensional materials. Adv Mater. 2014;26:992–1005. https://doi.org/10.1002/adma.201304138.

© STM Journals 2025. All Rights Reserved

24. Zhang H, Wang L, Chen Q, Li P, Zhou A, Cao X, et al. Preparation, mechanical and anti-friction performance of MXene/polymer composites. Mater Des. 2016;92:682–9. https://doi.org/10.1016/j.matdes.2015.12.084.
25. Zhou X, Guo Y, Wang D, Xu Q. Nano friction and adhesion properties on Ti3C2 and Nb2C MXene studied by AFM. Tribol Int. 2021;153:106646. https://doi.org/10.1016/j.triboint.2020.106646.
26. Huang S, Mochalin VN. Understanding Chemistry of Two-Dimensional Transition Metal Carbides and Carbonitrides (MXenes) with Gas Analysis. ACS Nano. 2020;14:10251–7. https://doi.org/10.1021/acsnano.0c03602.
27. Natu V, Hart JL, Sokol M, Chiang H, Taheri ML, Barsoum MW. Edge Capping of 2D-MXene Sheets with Polyanionic Salts To Mitigate Oxidation in Aqueous Colloidal Suspensions. Angew Chemie - Int Ed 2019;58:12655–60. https://doi.org/10.1002/anie.201906138.
28. Yan Z, Shi X, Huang Y, Deng X, Yang K, Liu X. Tribological Performance of Ni3Al Matrix Self-Lubricating Composites Containing Multilayer Graphene and Ti3SiC2 at Elevated Temperatures. J Mater Eng Perform. 2017;26:4605–14. https://doi.org/10.1007/s11665-017-2907-0.
29. Petrus M, Woźniak J, Cygan T, Lachowski A, Moszczyńska D, Adamczyk-Cieślak B, et al. Influence of ti3c2tx mxene and surface-modified ti3c2tx mxene addition on microstructure and mechanical properties of silicon carbide composites sintered via spark plasma sintering method. Materials (Basel). 2021;14. https://doi.org/10.3390/ma14133558.
30. Singh S, Han T, Chen X, Zhang C. Fabrication and assessment of dry sliding behavior of Ti3C2Tx-MXene reinforced nickel aluminide composites. Tribol Int. 2024;200:110131. https://doi.org/10.1016/j.triboint.2024.110131.
31. ASTM Standard E92-23. Standard Test Methods for Vickers Hardness and Knoop Hardness of Metallic Materials. ASTM Int West Conshohocken, PA 2023. https://doi.org/10.1520/E0092-23.
32. ASTM Standard G99-23. Standard Test Method for Wear and Friction Testing with a Pin-on-Disk or Ball-on-Disk Apparatus. ASTM Int West Conshohocken, PA 2023. https://doi.org/10.1520/G0099-23.

© STM Journals 2025. All Rights Reserved